Mühlnickel, Lukas; Jaurigue, Jonnel A.; Jaurigue, Lina C.; Lüdge, Kathy

The influence of timescales and data injection schemes for reservoir computing using spin-VCSELs

Original published in:	Communications physics. - London : Springer Nature, 7 (2024), art. 370, 12 pp.
Original published:	2024-11-14
ISSN:	2399-3650
DOI:	10.1038/s42005-024-01858-5
[*Visited:*	2025-04-11]

communications physics

Article

https://doi.org/10.1038/s42005-024-01858-5

The influence of timescales and data injection schemes for reservoir computing using spin-VCSELs

Check for updates

Lukas Mühlnickel, Jonnel A. Jaurigue, Lina C. Jaurigue & Kathy Lüdge

Reservoir computing with photonic systems promises fast and energy efficient computations. Vertical emitting semiconductor lasers with two spin-polarized charge-carrier populations (spin-VCSEL), are good candidates for high-speed reservoir computing. With our work, we highlight the role of the internal dynamic coupling on the prediction performance. We present numerical evidence for the critical impact of different data injection schemes and internal timescales. A central finding is that the internal dynamics of all dynamical degrees of freedom can only be utilized if an appropriate perturbation via the input is chosen as data injection scheme. If the data is encoded via an optical phase difference, the internal spin-polarized carrier dynamics is not addressed but instead a faster data injection rate is possible. We find strong correlations of the prediction performance with the system response time and the underlying delay-induced bifurcation structure, which allows to transfer the results to other physical reservoir computing systems.

Reservoir computing (RC) is a supervised machine learning technique where only the readout connections are trained via linear regression. This offers the unique possibility to use physical systems with a nonlinear response to perturbations to perform complex calculations. The first ideas of the concept date back into the 80s and 90s[1,2], being followed by the first fundamental algorithms, e.g. Liquid State Machine[3] and Echo State Network[4], and later on unified under the name RC[5]. A review about the history and recent developments of RC is given by Zhang et al.[6]. Due to their fast data processing and the relatively simple data injection and readout schemes, optical systems are especially suited and a variety of different optical RC implementations have already been proposed, theoretically investigated and experimentally realized[7,8].

It is well accepted that RC needs a high-dimensional response to the input in order to yield good performance[9]. We want to draw attention to the fact that for dynamical systems, it is also very important at which timescales and with which input perturbation these different phase space dimensions are addressed (i.e. which data injection scheme is chosen). We illustrate this using the dynamic response of vertical cavity semiconductor lasers (VCSELs) with two mode emission due to two separate charge-carrier sub-populations (spin-VCSELs) and with delayed optical self feedback. Spin-VCSELs are energy efficient and very fast electro-optical components[10–13], which are well suited for optical neuromorphic computing with a small footprint[14,15]. Due to these lasers having two carrier-populations with different spins, and the two cavity modes with different polarizations, they are dynamically complex and are suitable for various electrical or optical data injection methods. We want to utilize these aspects to demonstrate the crucial role of the underlying complex system dynamics for RC. Specifically, we want to discuss when and how additional dynamic degrees of freedom of the dynamical RC system, in our case the spin-VCSELs, can be beneficial. A central point of the discussion will be the bifurcation structure and the response timescales of the dynamical system.

We focus on time-multiplexed RC[9], but our insights apply to RC with dynamical systems in general. The results do not apply for realizations based on nonlinear vector regression (known as next generation RC[16]) as there no physical system with internal dynamics is involved. After the first optical realizations of time-multiplexed optical RC systems[17–19], a lot of progress has been made as, for example, summarized in the review on hardware realizations[20]. Additionally, numerous theoretical works have deepened the understanding of delay-based RC and developed optimization methods[21–29]. Reservoir computing with delayed self-feedback and injection has been experimentally realized with conventional lasers[30,31] and with VCSELs[32,33]. In these experiments, a strong dependence on the injection parameters was observed but a clear trend could not be identified. Another laser system, the quantum cascade laser, was theoretically investigated in[34] and the role of the carrier dynamics was highlighted. Also, the performance of an RC setup with injection and feedback was improved by a mirror with additional carrier dynamics[35]. With our work we want to contribute to a systematic

Technische Universität Ilmenau, Institut für Physik, Weimarer Straße 25, 98693 Ilmenau, Germany. e-mail: lina.jaurigue@tu-ilmenau.de; kathy.luedge@tu-ilmenau.de

understanding of all the different optical RC systems and provide a path toward predicting the computational abilities of physical reservoirs.

The potential of spin-VCSELs for time-multiplexed reservoir computing was already explored experimentally[32,33,36–38] and numerically for phase injection[39–46], but a complete picture and a structural understanding is still missing. We address these issues by analyzing the impact of the underlying nonlinear dynamics. Of particular importance, we show that regarding discussions about the best performance at the edge of bifurcations[47,48], care has to be taken when the input data itself induces small changes to the bifurcation structure. In order to reach good performance, general synchronization[49,50], i.e., a consistent response to the input, is needed. However, not only the operation parameter but also the input itself changes the system response. To demonstrate this point, we compare two different injection schemes and show how both utilize different aspects of the internal dynamics of the optical RC system.

Besides utilizing the bifurcation structure for parameter tuning, there are other ways to improve the performance of a RC setup, e.g. by means of state matrix extensions[28,51–54], input delay[54–56], additional nonlinear regression at the output[16,57], or the addition of physics informed information[58,59]. These methods are not the focus of the present study, but are complimentary to the work we present.

The main message of this paper is that a comprehensive understanding of the bifurcation structure of the dynamical system being used as the reservoir, along with the knowledge of the internal timescales and data injection scheme, is necessary in order to utilize the dynamical system's full potential for RC applications. Our results show that it is important to consider how information is fed into the reservoir in order to find regions of optimal performance. We do not claim to be able to predict what the regions of optimal performance for arbitrary task are, however, we shed light on another piece of the puzzle. There are two main ingredients to solving reservoir computing tasks: Nonlinearity and memory. While the memory can be moved to the input or output layers, the nonlinear transformation of the input data depends on the reservoir which, as we emphasize, is strongly influenced by the data injection method.

Results

For the delay-based reservoir computing setup chosen here, with a spin-VCSEL as the photonic reservoir (see Fig. 1), we show that the internal charge-carrier dynamics, the injection time scales and also the physical data injection scheme play a crucial role. The reservoir computing is implemented by calculating the time dependent light intensities of the two modes $I_+(t)$ and $I_-(t)$ after leaving the spin-VCSEL cavity (experimentally this corresponds to measurements with photo detectors). These values are used as entries for the state matrix which is multiplied with the weights to yield the output of the reservoir computer for a certain input (more details are described in the Methods section). The output weights are determined during the training process via linear regression. Once the RC is trained, in our case trained to predict the chaotic Lorenz-x time series one step into the future, the prediction performance of the optical RC system is determined by evaluating the normalized root mean square error (NRMSE) between target and output. We have chosen this Lorenz task as it does not require much memory[54] and therefore allows us to investigate the influence of the spin-VCSEL dynamics on the nonlinear transform capabilites of the reservoir. For tasks requiring memory on time scales of multiple clockcycles, memory inducing effects can be incorperated in the input or output layers[51,54,56,60].

Figure 2 shows scans of the spin-VCSEL dynamics as observed at the output facet without data injection (panel a) and its chaotic time series prediction performance after training (panel b) plotted in the parameter plane of the optical injection intensity and frequency detuning. The numerical results have been obtained by integrating the rate equation model for the externally driven spin-VCSEL with an external self-feedback line (delay time τ) and with data injected into the spin-polarized charge carrier difference via the polarized pump current $P(t)$ (see Fig. 1 and Methods section). The 2-dimensional hyper-parameter plane for characterizing the performance in Fig. 2 is chosen to allow for visualizing the bifurcation scenario. The bifurcation structure also changes with the feedback parameters and sensitively depends on the feedback delay time, feedback phase and feedback strength, similar to what is known for semiconductor lasers with injection and feedback[61–65] (which we will also briefly discuss later in this section). The reservoir computing specific parameters, such as virtual node distance and regularization parameter, do not change the bifurcation structure, but they have to be adjusted for different operation conditions in order to reach optimal performance (see Methods section).

For the optically injected spin-VCSEL without additional RC input (Fig. 2a), different emission dynamics can be observed; in the white area the laser is injection locked and emits light with constant intensity, while periodic oscillations (light blue) and complex dynamics (red colors) are observed outside the locking region (please see e.g. ref. 65 for a more detailed discussion of laser dynamics with injection and feedback). In Fig. 2b the chaotic timeseries prediction performance for data injected via the charge carriers is shown, and directly correlates with the dynamic behavior depicted in Fig. 2a. Good performance (dark green regions) is found within the area of stable constant wave emission (locking area) while outside the locking region no prediction is possible. The best performance for the carrier injection scheme, NRMSE = 0.002, is found close to the unlocking transition

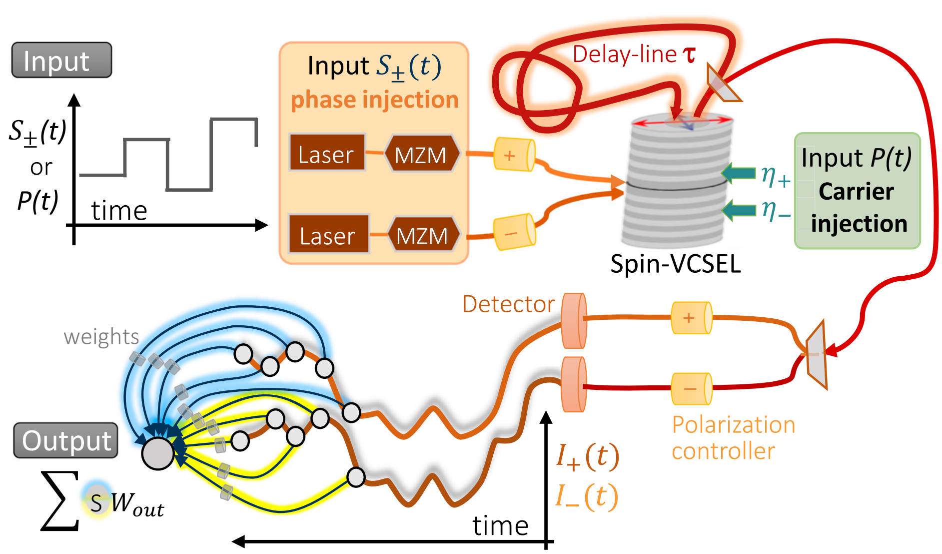

Fig. 1 | Spin-VCSEL based time-multiplexed reservoir computer. The spin-VCSEL is fed with time dependent input data which can be injected either via the phase of the injected light $S(t)$ (MZM are Mach-Zehnder-modulators), or electrically by varying the spin polarized carrier densities via $P(t)$. The intensities of the two polarizations (I_- and I_+) are read out at several points in time and added together via a weighted sum, the weights are determined via linear regression. Delay length τ, injection strength, injection frequency and feedback strength can be varied.

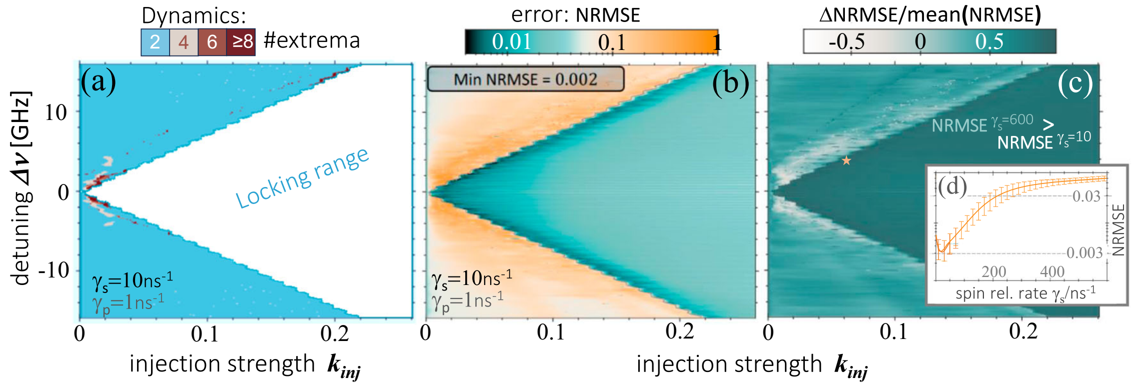

Fig. 2 | Dynamics and performance for carrier injection in parameter space (k_{inj}, $\Delta\nu$). **a** Dynamics of the Spin-VCSEL without data injection color coding the distinct extrema observed in the time evolution of the intensity $|E_+|^2$, white indicates stable constant wave emission (locking range) while blue indicates periodic oscillations. **b** Computing error (Lorenz-63 x-prediction, 0.1 step ahead) plotted via color code with data injection into the spin polarized carriers, spin relaxation rate $\gamma_S = 10$ ns^{-1}. **c** Normalized difference (NRMSE$_{600}$-NRMSE$_{10}$) between the NRMSE error for normal (panel **b**) and high spin relaxation rates ($\gamma_s = 600$ ns^{-1}), dark colors indicate a strong impact of γ_S on the performance, **d** shows the performance as a function of γ_S taken at the locking boundary (star in **c**) with error bars indicating the standard deviation after using 30 different masks. Parameters as in Table 1, $\gamma_P = 1$ ns^{-1}, Feedback strength $k = 0.0022$.

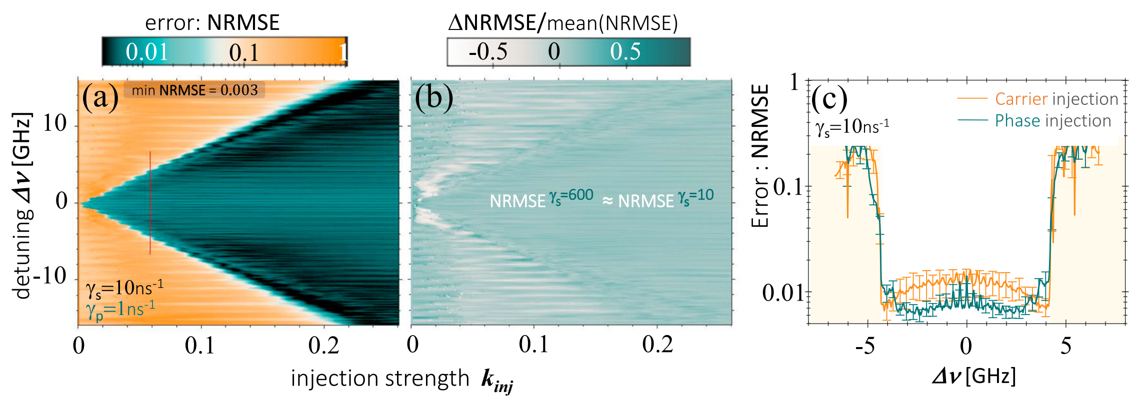

Fig. 3 | Performance for phase injection. **a**, **b**: same as Fig. 2b, c but for data injection into the phase, red line indicates line scan shown in **c**. Light colors in **b** indicate no effect of changing the spin relaxation rate. **c**: line scan along varying detuning at $k_{inj} = 0.059$ showing performance for carrier (orange line) and phase injection (green line), error bars show standard deviation after using 30 different masks, yellow shaded regions are outside the locking region. Parameters as in Table 1, $\gamma_P = 1$ ns^{-1}, Feedback strength $k = 0.0022$.

line. In the literature, e.g. refs. 36,43,66, different trends have been observed for the dependence of the RC performance on the detuning, however there phase injection was used, which makes a difference as we discuss later in this section. The carrier injection used in Fig. 2 induces the nonlinear response to the input directly in the difference of the spin-polarized charge carriers m, which is most complex close to the unlocking transition. Since data injection into the carrier dynamics does not significantly shift the bifurcation lines, the bifurcation structure of the spin-VCSEL reservoir without data injection can be used to find the regions of good RC performance.

To demonstrate the effect of the spin polarized charge carrier dynamics, which sets the spin-VCSEL apart from regular semiconductor lasers, we tune the timescale at which they equilibrate. In our case this can be done by changing the spin relaxation rate γ_s. Figure 2c shows the changes in performance for the case that the spin relaxation rate, which was $\gamma_s = 10$ ns^{-1} in Fig. 2b, is tuned to a very high value of $\gamma_s = 600$ ns^{-1}. A scan in γ_S can be seen in the inset in panel (d). It was taken at the locking boundary (star in panel(c)) and the continous degradation with increasing spin relaxation rate is obvious. As can be seen by the colors in Fig. 2c, a strong decrease of the performance is observed throughout the complete locking region (dark green colors). The reason is that for the very fast spin decay rates ($\gamma = 600$ ns^{-1}), the variable m describing the difference of the spin polarized carrier populations instantaneously follows the input and is not contributing with an additional dynamical response. Thus, the $m(t)$ that enters the field equation in this limit is just the sample and hold version of the input (with a scaling factor that depends on the other variables). We therefore only reach performance values of 0.04 which are similar to the limit where the dynamical system is described by a map[56], i.e. where the dynamics and the memory is solely introduced by the delayed feedback term. In the case of small $\gamma_s = 10$ ns^{-1}, a complex nonlinear response with a memory of different inputs (due to inertia of m) enters the field equation and the resulting nonlinear mixing leads to performances that are by an order of magnitude better (0.003). Different RC tasks will have different requirements for memory and nonlinearity, as was e.g. shown in refs. 54,67. Nevertheless, the parameter regions where the internal charge-carrier dynamics contributes best to the reservoir performance with carrier injection is task independent.

Different injection schemes

As mentioned before the specifics of the chosen perturbation of the dynamical system, i.e. the specifics of the data injection scheme, plays an important role for the RC performance. To highlight that we now repeat the analysis with a different injection scheme; the much more common phase injection scheme where two Mach-Zehnder modulators are used to change the phase of the injected light (Fig. 1). The results are plotted in Fig. 3 (same parameter plane color code as in Fig. 2b). The most striking difference is the fact that the best performance is no longer found at the borders but shifted

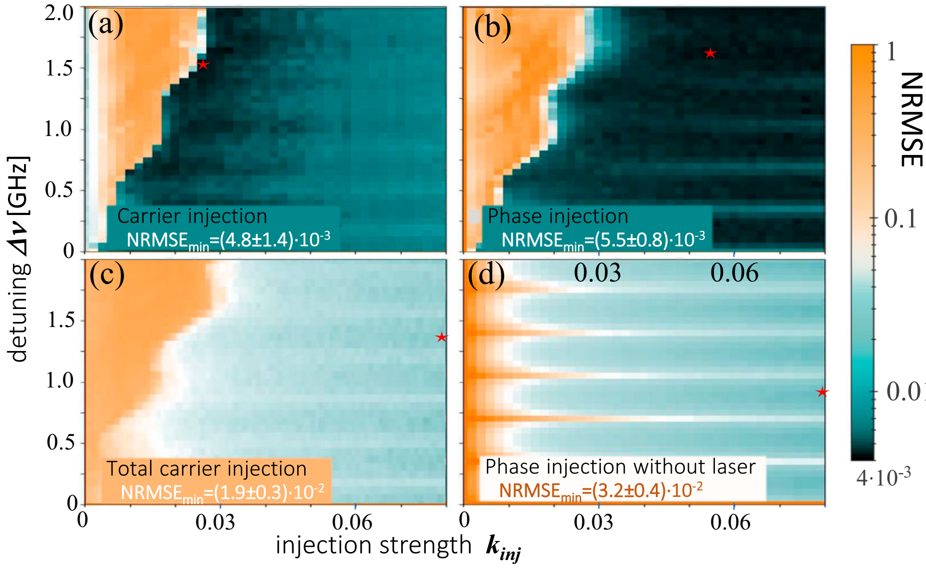

Fig. 4 | Comparison of prediction performance with different injection schemes. a Carrier injection where data is injected into the difference of spin polarized charge carriers m, **b** phase injection, **c** injection into the total carrier density N, and (**d**) phase injection into an optical setup without a VCSEL leaving only the detector nonlinearity. Color codes the prediction error (NRMSE) as given in the color bar. The red star marks the best performance in each panel (values given as insets). Parameters as in Table 1, $\gamma_p = 1\ \mathrm{ns}^{-1}$, $\gamma_s = 10\ \mathrm{ns}^{-1}$.

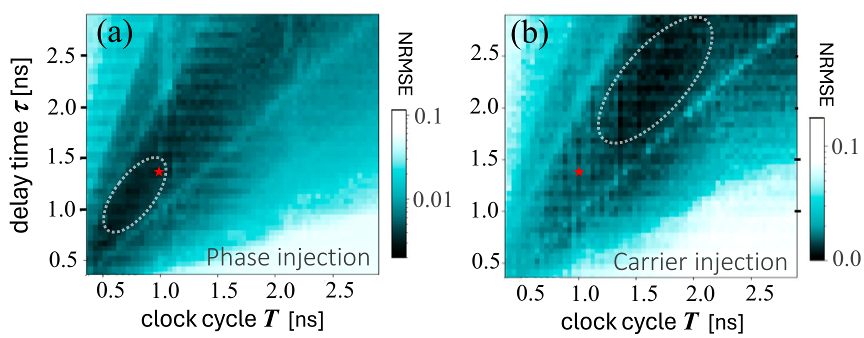

Fig. 5 | Impact of input timescales. Performance for phase (a) and carrier (**b**) injection in the RC parameter space spanned by clock cycle T and delay time τ at $k_{inj} = 0.22$, $\Delta\nu = 14$ GHz. Color codes prediction error. Red star mark values used in Figs. 2–4; Dashed ellipse highlights optimal performance regions. Parameters as in Table 1, $\gamma_P = 1\ \mathrm{ns}^{-1}$, feedback strength $k = 0.0022$.

into the locking region. The RC system itself was not changed, thus, the unperturbed bifurcation structure (without RC input) is identical to Fig. 2a. Decent performance with phase injection is also found within the locking region, however modulated by horizontal stripes which result from the external cavity modes induced by the external feedback[61,68,69]. The difference between the two injection schemes is the dynamical perturbation by the input data. For the carrier injection, the perturbation first has to be dynamically coupled to the light intensity, while it directly perturbs the complex valued light field in the phase injection case. The nonlinear transformation of the input is therefore already happening in the field equation and the coupling to the carriers is not the dominating effect.

Figure 3c shows a line scan of the performance as a function of the frequency detuning between the spin-VCSEL and the injection laser (the position is indicated by a red vertical line in Fig. 3a). Two things have to be noted here. First, the optimal detuning depends on the data injection scheme, and second, optimization is difficult if only one parameter is tuned. Comparing the two 2-dimensional scans Figs. 2b and 3a, it becomes clear that the effect of the injection strength k_{inj} is different in both cases. While a higher k_{inj} is always beneficial with phase injection, it deteriorates the performance in the carrier injection case. Although this result seems to contradict the common rule of best performance close to bifurcations (also known as *the edge of chaos* in the literature), it does not when the effect of the data injection on the bifurcation structure is taken into account. The phase injection directly changes the intensity of the light entering the spin-VCSEL cavity and thus also slightly changes the bifurcation lines in the parameter plane (these changes are small as long as the RC input is a small perturbation). As a result, being close to the unperturbed bifurcation does not ensure staying within the locking region (in contrast to carrier injection). Instead the regions of best performance are slightly shifted from the edges into the locking region.

When the data is injected via the optical phase, the light intensity is directly modulated by the input data, therefore the role of the spin relaxation timescale and thus the role of the charge-carrier dynamics is changed compared with data injection via the spin polarized carriers. Figure 3b depicts the difference in the performance between a phase injected spin-VCSEL with high and low spin-relaxation rates (compare Fig. 2c). It can be seen that the difference in the performance of the two lasers is negligible (light green colors in Fig. 3b) as changes in m are only indirectly induced by the input. In order for the dynamic degree of freedom of m to be addressed by phase injection, the perturbation in $I_{\pm}$ has to be coupled to m and then coupled back to the field (see differential equation system Eq. (1)).

To check how much the active laser material, i.e. the nonlinear light-matter interaction between the light and total charge-carrier number within the spin-VCSEL, contributes to the RC performance with phase injection, we eliminate the laser and replace it with a passive cavity. In this case the only nonlinear elements are the Mach-Zehnder modulators, the delay and the quadratic detection at the photo detectors. The performance for this passive case is plotted in Fig. 4d together with the injection schemes discussed before (Fig. 4a, b) and the case where the data is injected into the total carrier density N (Fig. 4c). The first thing to notice is that a decent performance is already possible with phase injection into a passive-cavity-setup (NRMSE of 0.03 in Fig. 4d), but the best performance possible is a factor of 6 worse than for the cases with the VCSEL inside the cavity (Fig. 4b). Thus, for phase injection the interaction with the total carrier dynamics is crucial but the interaction with m is negligible (because eliminating m with fast γ_S has no effect as shown in Fig. 3). An injection into the total carriers (Fig. 4c) reaches

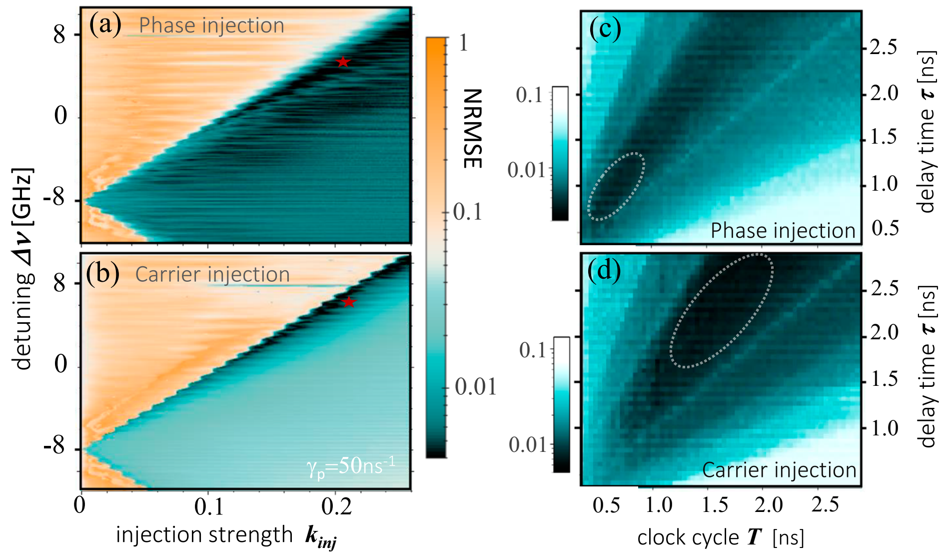

Fig. 6 | Prediction error for high birefringence $\gamma_p = 50\ \mathrm{ns}^{-1}$. **a** and **b** show results within the injection parameter plane (k_{inj}, $\Delta\nu$) for phase- and carrier injection while **c** and **d** show results within the reservoir parameter space (τ, T) at $k_{inj} = 0.22$, $\Delta\nu = 4$ GHz as indicated on the left with the red stars. Dashed ellipse in **c** and **d** highlight optimal performance regions. Color codes the prediction performance as indicated by the color bar. Parameters as in Table 1.

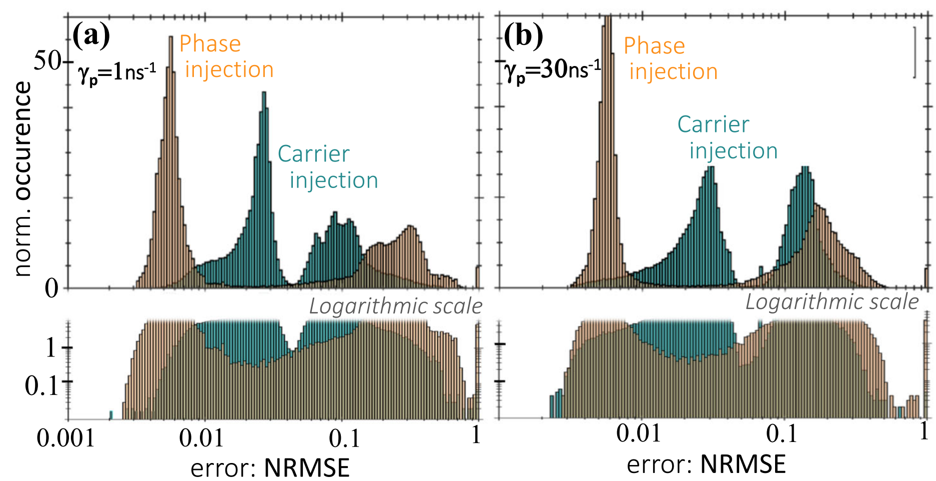

Fig. 7 | Statistics within injection parameter space. **a** Histogram of the computing performance observed within the locking cone of the 2-dim. parameter scan (k_{inj}, $\Delta\nu$) for carrier (green) and phase injection (orange) shown in Figs. 2b and 3a. **b** Same as **a** but for higher birefringence $\gamma_p = 30\ \mathrm{ns}^{-1}$ (2-dim. NRMSE scan for $\gamma_p = 30\ \mathrm{ns}^{-1}$ can be found in Supplementary Note 1, Supplementary Fig. 1).

only slightly better values than the passive cavity. Here, the dynamics of the spin polarized carriers is not addressed and both modes get the same input via N. Thus only the relaxation oscillation between total carriers and field yield memory and nonlinear mixing. Since N evolves on a very slow timescale ($\gamma = 1\ \mathrm{ns}^{-1}$) this nonlinear interaction is less effective than what can be reached via data injection into the spin polarized carriers (Fig. 4a).

Passive cavities have been used in previous works, e.g. on micro-ring resonators with feedback, where reservoir computing was experimentally demonstrated[70] and it was numerically shown[71] that, depending on the task, the nonlinearity induced by the photo detection can already be sufficient for decent time series prediction. We can support this results but we also state that utilizing additional dynamics that evolve on a timescale where the system is sampled, will improve the computing results (compare passive cavity in Fig. 4d with the active cavity in panel (a) and (b)). Another suggestion for a minimal reservoir formed only by a MZM with delay and without dynamic component was given in ref. 72 and ref. 73. Nevertheless, as we show here, adding an active nonlinear component like the spin-VCSEL leads to an improvement of the computing ability by at least one order of magnitude.

Role of Input timescale

So far our results were based on constant, well chosen values for the feedback delay τ and the virtual node distance θ. To visualize the impact of the input timescale and to underline their importance, we provide scans of the performance in the ($\tau - T$)-parameter plane in Fig. 5 (taken within the locking region of Fig. 2). Good performance (dark regions) is reached along the diagonal for $\tau \approx 1.4T$. Similar relations have been seen before in other RC systems[24,74]. If carrier and phase injection results are compared in the two panels Fig. 5a and b it can be seen that the carrier injection scheme is better at slower injection rates $1/T$ (larger virtual node distance θ) while phase injection performs well at smaller T (small θ). Overall a relatively wide range of T values performs well.

If processing speed is an issue for a specific application, the phase injection scheme will outperform carrier injection by a factor of 3. For the injection parameter scans presented before we used values where both injection schemes perform well, i.e. we use a ratio of $\tau/T = 1.41$ and we chose $T = N_V \cdot \theta = 30 \cdot 33$ ps = 1 ns. If comparing Fig. 5a, b the phase injection has overall much better performance. The reason is that we chose similar values for the injection parameters that lie well within the locking region. Carrier injection performs better at the unlocking border (see Fig. 2) but there a scan in τ is not sensible as it leads to a periodic shift of the locking boundary (see Supplementary Note 3, Supplementary Fig. 4 for details of the bifurcation structure).

For every dynamical system used for a RC setup, the best value for T is determined by the characteristic response time. However, as we discussed above, this time not only depends on the system itself but also on how the

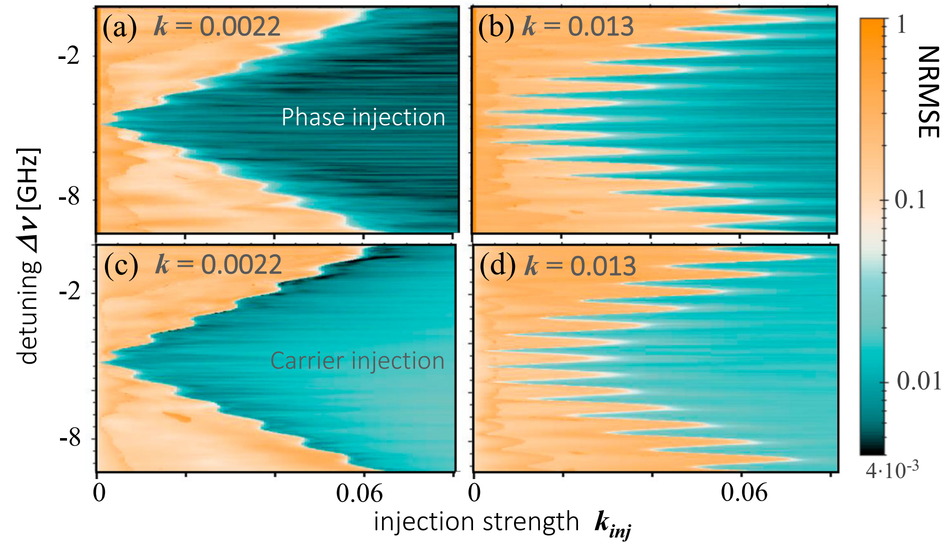

Fig. 8 | Impact of feedback strength *k*. Color coded prediction error (NRMSE) for phase injection (**a**, **b**) and carrier injection (**c**, **d**) with $\gamma_p = 30\,\mathrm{ns}^{-1}$ in the injection parameter space (k_{inj}, $\Delta\omega$) for $k = 0.0022$ (**a**, **c**) and $k = 0.013$ (**b**, **d**). Parameters as in Table 1.

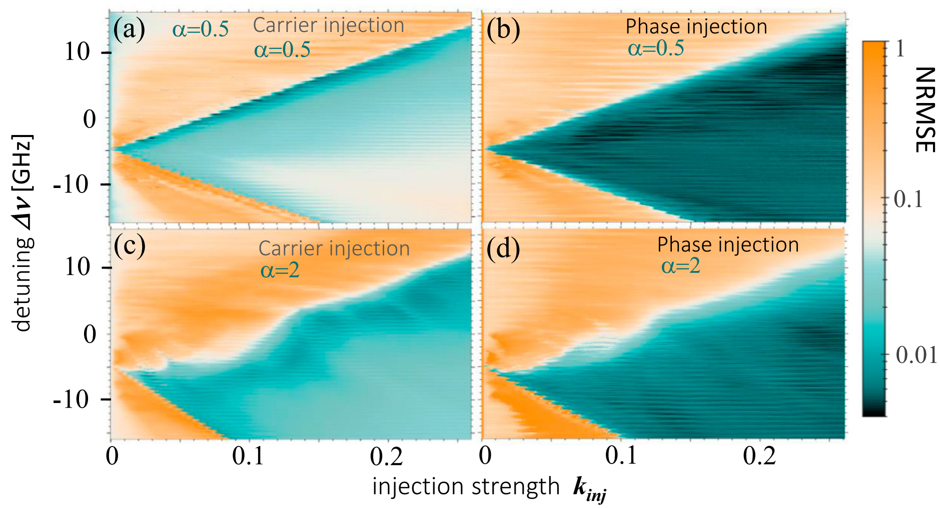

Fig. 9 | Impact of linewidth enhancement factor *α*. Color coded prediction error (NRMSE) for carrier (**a**, **c**) and phase injection (**b**, **d**) with $\gamma_p = 30\,\mathrm{ns}^{-1}$ in the injection parameter space (k_{inj}, $\Delta\omega$). (**a**, **b**): $\alpha = 0.5$, (**c**, **d**): $\alpha = 2.0$. Parameters as in Table 1.

system is perturbed. For our example, information that is injected into the carriers decays at a slower rate than a perturbation applied to the phase. The latter is especially fast in the chosen spin-VCSEL laser.

It is important to note that a change in T always has to be accompanied by a change in the chosen delay time in order to optimally match the memory of the system with the requirements of the task. Other tasks will need different memory and thus other optimal values for the ratio between T and τ.

Impact of birefringence

After having understood the impact of the spin polarized carrier relaxation dynamics and the impact of the data injection scheme, we want to explore to what extend the birefringence parameter γ_P changes the bifurcation scenario and the performance. Tuning the birefringence leads to changes in the modulation response due to the occurring polarization oscillations[11] and it has been shown that higher values drastically increase the modulation speed possible with those lasers[12,75]. To visualize the impact of γ_p on the computing performance, 2-dim. parameter scans for a higher birefringence value of $\gamma_p = 50\,\mathrm{ns}^{-1}$ are shown in Fig. 6a, b for phase and carrier injection, respectively. The first thing to notice is a shift of the complete locking tongue to lower detuning frequencies with higher birefringence (compare Figs. 2 and 3), which is related to a frequency shift of the emitted light of the spin-VCSEL with γ_P which then consequently shifts the frequency region where it is resonant to the injecting light. The distribution of good performance regions within the locking cone is similar to the case for low birefringence. Only the overall best performance increases slightly for higher birefringence and the best operation parameters shift to higher injection strengths (dark green colors in Fig. 6a, b).

As discussed before for lower birefringence, the two injection schemes differ in their optimal value for the data injection rate T due to the different perturbations and the resulting different nonlinear response. The ($\tau - T$)-scans presented in Fig. 6c, d visualize again that phase injection works best at small $T = 0.5$ ns with a corresponding node distance of $\theta = 17\,ps$ and can therefore work at faster data injection rates.

To better quantify the distribution of performance values in the injection parameter plane, we plot the respective histograms for both injection schemes in Fig. 7. As already expected from the color distribution in the 2-dim. plots in Figs. 2b and 3a, the phase injection (orange bars) covers larger areas of good performance while the carrier injection (green bars) provides the best values (only visible in the logarithmic zoom in the lower row). With larger birefringence (Fig. 7b), the peak of the error distribution at small values becomes more narrow and shifts slightly to the left.

Impact of Bifurcation structure

The last part of our discussion is devoted to the impact of other parameters of our laser setup, i.e. the feedback strength k and the linewidth enhancement factor α. With this we want to underline the importance of the bifurcation structure and thus the importance of a careful investigation of the physical system before its reservoir computing performance is quantified. In Fig. 8, two values for the strength of the delayed feedback k are compared (left and right column). The small saw tooth features at the edge of the locking region, which are due to locking with other external cavity modes[68,69,76], are much more pronounced for large k (panel b and d). The bifurcation lines also change when the phase of the injected light, which explains why the performance within these teeth for the phase injection (upper row) is worse than in the middle of the locking cone. Close to the teeth the data injection causes small shifts of the locking boundary and can therefore drive the laser into the region of complex dynamics. For carrier injection (lower row), overall a degradation of the performance is observed for higher k, presumable because the strong field interactions with the external cavity modes are dominating and the system is not susceptible any more to perturbations in the carrier dynamics.

The performance of our spin-VCSEL RC for different values of the α-factor is presented in Fig. 9. Here, a very different modification and reshaping of the bifurcation structure is observed (as expected from previous results about the impact of the α-factor on the bifurcation structure of injection locked lasers[77,78]). The more complex dynamics induced by an α-factor larger than 0.5 is not beneficial and deteriorates the performance. One reason could be the beating between the different external cavity modes that occurs for α-factor larger than 1[79].

The dramatic change in the bifurcation structure and the change in the distribution of good performance values within the injection locking parameter space underlines again the importance to understand the dynamical system first before judging its RC suitability.

Lastly, it is noted that the choice of the delay time τ changes the bifurcation structure (it determines the distance of the saw tooth like looking tongues[65]) and larger τ increases the level of multistability[62,79,80]) which is related to the bifurcation structure and will be true for every task at hand. Tuning the delay τ will shift the locking boundary and can consequently shift the operation point into the bad performing region with complex oscillations for the case that the operation point was close to the locking boundary. Additionally, the ratio between τ and T changes the performance due to resonance effects[24,25,67] and due to the influence on the memory of the reservoir[54,67] (compare also Fig. 5, Fig. 6c, d).

Conclusion

Using the example of a spin-VCSEL reservoir, we have shown that the injection scheme and the strength of the perturbation induced by the input data play an important role and can change the behavior in parameter space. In our example, data injection via a modulated phase slightly changes the locking boundary of the laser system and can thus drive the system out of stable operation regime if it is operated close to the unlocking transition. Therefore, the unperturbed bifurcation line is not a good operation point. In contrast to that, the behavior is very different for data injection via the charge carrier difference, which is possible via spin polarized pump current injection. In this case, the nonlinear dynamics is induced in the carriers and the bifurcation line in the injection parameter space does not change. Consequently, for this case the best performance is found at the border to the unlocking transition (also referred to as *edge of stability*). We emphasize that the change in the optimal parameter region arises due to the difference in the dynamical response of the reservoir when data is injected either via the phase or the charge carrier difference, not due to the task we have used to demonstrate our results.

We thus conclude that by exploring the underlying bifurcation structure of a dynamical system prior to its application as a reservoir computer, seemingly contradictory behavior found experimentally in different parameter regions can be resolved and optimization becomes much easier.

For the spin-VCSEL the birefringence parameter and the linewidth enhancement factor have the most impact on the bifurcation structure. While large birefringence improves the best value that can be reached with the RC, a high amplitude phase coupling is not found to be beneficial. Both parameters shift and deform the locking regions such that care has to be taken when adjusting the hyperparameter.

For every laser system that is used for the RC setup investigated here, the internal carrier decay timescales are important. The reason is that the data induced perturbation has to be coupled to the measurable quantity. If the perturbation decays before the dynamic coupling to the measured quantity can happen, the reservoir loses an additional source of memory and nonlinear mixing and therefore performs worse. If carrier injection via the spin polarized pump current is chosen, the spin carrier equilibration time is crucial for the nonlinear mixing of the information. However, this dynamic degree of freedom is not addressed for the case of data injection via the phase.

The bifurcation analysis and thus the hyper-parameter optimization of the time-multiplexed reservoir computing approach discussed here was done within the injection parameter space. If our results are compared to results presented in[43] and[66], where laser with injection and feedback are used for RC applications, we can now explain why the best consistency was not found at the edges of the unlocking transition. The reason is the injection scheme. If phase injection via Mach-Zehnder modulators is used, good performance is found within the whole locking region up to high injection strengths. On the contrary, for carrier injection, which can be realized via spin polarized currents, there is only a small area at the edge of the locking region where best performance is reached.

In general, to optimally use the dynamical degrees of freedom of a physical reservoir, the specific response to perturbations from data input has to be taken into account, especially when there are processes within a reservoir which evolve at very different timescales.

Methods

Rate equation model for spin-VCSEL

For our numerical simulations we use the Spin-Flip-Model derived in refs. 81,82 and simulate the time dependent dynamics of the light field within the externally perturbed spin-VCSEL. The electric field inside the cavity is polarized either right circular (E_+) or left circular (E_-). The total sum of the charge carrier sub-populations is given by N, while m describes their difference:

$$\begin{aligned}\frac{\mathrm{d}}{\mathrm{d}t}E(t)_\pm &= \kappa(1+i\alpha)(N\pm m-1)E_\pm - (\gamma_a + i\gamma_p)E_\mp \\ &\quad + 2k\kappa E_\pm(t-\tau)e^{-i\phi} \\ &\quad + \kappa k_{inj}|E_0|(1+e^{iS(t)_\pm})e^{2\pi i\Delta\nu t}\end{aligned} \tag{1}$$

$$\begin{aligned}\frac{\mathrm{d}}{\mathrm{d}t}N(t) &= \gamma\big[\eta - N(1+|E_+|^2+|E_-|^2) \\ &\quad -m(|E_+|^2-|E_-|^2)\big]\end{aligned} \tag{2}$$

$$\begin{aligned}\frac{\mathrm{d}}{\mathrm{d}t}m(t) &= \gamma\eta P(t) - [\gamma_s + \gamma(|E_+|^2+|E_-|^2)]m \\ &\quad - \gamma(|E_+|^2-|E_-|^2)N.\end{aligned} \tag{3}$$

Here, κ is the field decay rate, α is the linewidth enhancement factor, γ_a the linear dichroism, γ_p describes birefringency, γ the carrier decay rate, γ_s the Spin-Flip rate and η the total pump current normalized to threshold. The excess in the decay rate γ_s over γ accounts for the mixing of the carriers with opposite value of J_z[82]. Because similar inputs should result in equivalent system reactions, γ_a was set to 0, to avoid unilateral threshold reduction. This SFM rate equation model for a spin VCSEL has been intensively

Table 1 | Simulation parameters

Symbol	Value	Symbol	Value	Symbol	Value
Photon decay rate 2κ	460 ns^{-1}	Solitary laser field E_0	0.5		
Birefringence γ_p	1 ns^{-1}	Injection strength k_{inj}	0… 0.25	Total pump η	1.5
Spin relaxation rate γ_s	10 ns^{-1}	Feedback strength k	0.0022	Regularization λ	10^{-10}
Alpha factor α	0	Feedback phase ϕ	0	Virtual nodes N_v	30
Electron lifetime γ	1 ns^{-1}	Inputscaling (Carrier) G_C	0.05	Clock cycle T	1 ns
Linear dichroism γ_a	0 ns^{-1}	Inputscaling (Phase) G_P	0.1	Delay time τ	1.41 ns

investigated regarding their steady states and stability properties, see e.g. refs. 82–85. According to those results we choose an electric pump electric current of η = 1.5 below the first instability threshold and yields stable cw emission of the spin-VCSEL without external perturbations. The value of η measures the sum of the two pump currents into the two spin polarized sub-populations η_+ and η_-.

The complete setup for the RC system is visualized in Fig. 1. The spin-VCSEL is optically injected by two laser beams with controlled polarization. The phase and the intensity of each injecting beam is controlled via a Mach-Zendner-Modulator(MZM). A portion of the electric field in the VCSEL cavity is fed back to the VCSEL after a round-trip time τ, while a setup of beam-splitters and polarization controllers allows the measurement of the intensity of the two polarizations $I_\pm(t)$ as a function of time. The feedback term (second line in Eq. (1)) includes k as the dimensionless feedback strength, τ measuring the external round-trip time and a phase difference ϕ between the field exiting the spin-VCSEL and the field re-entering after one round trip. This term is equivalent to the feedback term originally introduced by Lang and Kobayashi[61]. Its effect on the dynamics of a single mode semiconductor laser has been widely explored[64,68,86,87]. For our two-mode VCSEL, both modes are fed back into the cavity.

$P(t)$ corresponds to the polarization of the pump current, i.e. $P(t) = (\eta_+ - \eta_-)/\eta$, and will be used for our time depended carrier injection method thereby directly changing the change in m. It is experimentally possible either via optical absorption of polarized light or via electrical injection of spin polarized carriers (i.e. via η_+ and η_-). If carrier injection is not used we set P = 0. The optical injection via the Mach-Zehndner-Modulators (MZM) is described by the third line in Eq. (1), where k_{inj} is the injection strength, $|E_0|$ the VCSEL intensity without injection and $\Delta\nu$ the frequency detuning between rotating frame and injection laser frequency. $S_\pm(t)$ corresponds to the polarization depended phase-shift induced in one arm of the MZM resulting in an effective intensity and phase modulation (both MZM can be addressed separately, allowing for polarization specific inputs which has been experimentally demonstrated in ref. 36 or in ref. 32 for one injecting laser). The effect of optical injection (without additional data input) on semiconductor lasers has been widely studied, see e.g. refs. 77,88–92. The effect of a combination of feedback and injection on the bifurcation structure is less studied but works exist for conventional semiconductor lasers[62,76] and quantum-dot lasers[65].

If data injection via the phase is modeled, $S_+(t)$ and $S_-(t)$ are both time dependent, else they are both set to 0. The latter results in a constant injection amplitude of $2kk_{inj}|E_0|$. The factors are chosen such that it gives a dimensionless injection strength k_{inj} where a value of k_{inj} = 1 means injecting with an amplitude per cavity lifetime that is equal to $|E_0|$. As mentioned before, the spin-VCSEL itself is driven by an electrical pump current that is described via η. If data injection into the total carrier density N is to be modeled, η becomes time dependent.

The Eqs. (1)–(3) were solved using a 4^{th}-order Runge-Kutta method with Hermit interpolation and an interpolation step of $1ps$. The material related parameters for the spin-VCSEL were taken from[43] and given in Table 1 together with all RC relevant parameters. The dynamics of the spin-VCSEL setup without data injection (with $S_\pm$ = P = 0) was characterized by counting the number of extrema within one period. Constant wave (cw) emission in Fig. 2a show 1, while e.g. for regular periodic oscillations 2 and for complex intensity pulsations values larger than 6 are found.

For large spin relaxation rates γ_s, the two laser fields $E_\pm$ are only coupled to the total carrier population N, which describes a dual-polarization VCSEL. A very small value, i.e. the minimal value is given by $\gamma_s = \gamma$, leads to a decoupling of the two modes if birefringence is absent. These limits are explored in our paper to figure out the impact of this characteristic timescale in comparison to the other dynamical timescale within the spin-VCSEL.

Reservoir computing and state matrix

A reservoir computing setup can be realized with a physical system, in our case the spin-VCSEL. For this, an input layer is needed to drive the system and an output layer in order to collect the nonlinearly transformed information. The output is collected into the state matrix $\mathbf{S}$. The weights $\mathbf{W}^{\text{out}}$ for the readout at the output layer are determined via linear regression by minimizing the distance to the target $\mathbf{o}$ as given in Eq. (4) (λ is the Tikhonov regularization parameter, a penalty term to avoid overfitting).

$$\min_{\mathbf{W}^{\text{out}}}\left(\| \mathbf{S}\mathbf{W}^{\text{out}} - \mathbf{o}\|_2^2 + \lambda \| \mathbf{W}^{\text{out}}\|_2^2\right) \tag{4}$$

The Tikhonov regularization parameter λ was optimized and set to 10^{-10} if not mentioned differently, $\mathbf{I}$ is the identity matrix. λ has the same effect as regularization by noise, where noise is added to the state matrix values (e.g. describing the effect of adding spontaneous emission noise).

The solution of Eq. (4) is given by $\mathbf{W}_{\text{out}} = \left(\mathbf{S}^T\mathbf{S} + \lambda\mathbf{I}\right)^{-1}\mathbf{S}^T\mathbf{o}$. The output of the RC system is then computed via $\hat{\mathbf{o}} = \mathbf{S}\mathbf{W}^{\text{out}}$ and the computation error in predicting the target $\mathbf{o}$ is quantified by the normalized root mean square error ($NRMSE$)

$$NRMSE = \sqrt{\frac{1}{N_I}\sum_{k=1}^{N_I}\frac{(\hat{o}(k) - o(k))^2}{\text{var}(\mathbf{o})}}. \tag{5}$$

that incorporates the normalization by the variance of the target var($\mathbf{o}$). N_I is the number of training or testing steps. For our prediction tasks the reservoir was trained with 10000 inputs and tested with 5000 data points.

$$\mathbf{S} = \begin{bmatrix} I_-(\theta) & I_-(2\theta) & \dots & I_-(N_V\theta) & I_+(\theta) & I_+(2\theta) & \dots & I_+(N_V\theta) & 1 \\ I_-(\theta+T) & & & & I_+(\theta+T) & & & \vdots & 1 \\ \vdots & & & & \vdots & & & \vdots & 1 \\ I_-(\theta+N_IT) & \dots & \dots & I_-(N_V\theta+N_IT) & I_+(\theta+N_IT) & \dots & \dots & I_+(N_V\theta+N_IT) & 1 \end{bmatrix} \tag{6}$$

In order to collect the non-linearly transformed information at the output layer, the state matrix $\mathbf{S}$ has to be filled. Since we are using a time-multiplexed approach, we feed in one data point per clock cycle T and read out the intensity of our two laser modes, $I_- = |E_-|^2$ and $I_+ = |E_+|^2$, at N_V time instances during one clock cycle T (this fills one line in the state matrix $\mathbf{S}$).

For all calculations, $N_v = T/\theta = 30$ virtual nodes were used. For the training (or testing) phase with N_I inputs, the state matrix $\mathbf{S}$ is given by Eq. (6).

Given a virtual node distance of $\theta = 33ps$, which we found to be a good choice for the spin-VCSEL, we obtain a clock-cycle of $T = 1\ ns$ for the data injection. This corresponds to a data processing rate of 1GHz. The value of θ strongly depends on the modulation response of the chosen dynamical system and needs to be adjusted if different dynamical systems (or hugely different parameters for the spin-VCSEL) are used.

The delay time τ of the external feedback loop was set to $1.41ns$ in order to avoid resonances with the clock cycle[24,67]. From our previous works we know that a ratio of $\tau/T \approx \sqrt{2}$ is usually a good choice[26,74]. However, we also provide detailed τ-T scans in the paper to visualize the importance of the ratio between these two timescales.

Input data and prediction task

A time continuous input data signal $J_{\pm}(t)$ is fed into the spin-VCSEL reservoir Eqs. (1)–(3) via the phase

$$S(t)_{\pm} = G_P \cdot J_{\pm}(t) \tag{7}$$

or via changing the pump polarization

$$P(t) = G_C \cdot J_{+}(t). \tag{8}$$

We call the first injection method *phase injection* while we refer to the latter as *carrier injection*. The two input scaling factors G_P and G_C are used as hyper parameters for optimization. The input signal $J_{\pm}(t)$ is constructed from time discrete task dependent input sequences in the following manner. Let $j_i(k)$ be a set of task dependent input data sequences running over the discrete time variable k. Then apply a sample and hold method (hold each $j_i(k)$ constant for the duration of one clock cycle T) to transform the inputs to continuous signals $j_i(t)$. Then multiply each signal with a mask signal $m^i_{\pm}(t)$ that repeats every T (the mask is analogous to an input weight matrix, its values are drawn from an i.i.d distribution between -1 and 1) and add the resulting terms together such that

$$J_{\pm}(t) = \sum_{i}^{N_J} m^i_{\pm}(t) j_i(t), \tag{9}$$

where N_J is the number of task dependent input signals.

In case of tasks that have input data of higher dimension (e.g. the Madelon task[93], spatio-temporal dynamics modeled by the Kuramoto–Sivashinsky equations[58], or chaotic dynamics described by all three Lorenz variables[58,94]) the same approach can be used. The only difference is a pre-processing step that transforms the higher dimension into a sequence of data in time via concatenation, thereby of course increasing the clock cycle (see e.g. ref. 94).

For training and testing the performance of our spin VCSEL RC system, we use the Lorenz 63 task, i.e. the prediction of one step into the future of the chaotic time series resulting from the Lorenz system. The Lorenz 63 system[95] is described by the three coordinates:

$$\dot{x} = \sigma(y - x);\ \dot{y} = x(\rho - z) - y;\ \dot{z} = xy - \beta z. \tag{10}$$

The parameters are chosen such that Eqs. (10) yield chaotic dynamics, i.e. we set $\sigma = 10$, $\rho = 28$, and $\beta = 8/3$. We integrate numerically with a Runge-Kutta 4th-order solver and a step size of $\Delta t_{sim} = 0.01$. The time series $x(t)$ was then sampled with a time step $\Delta_d = 0.1$ to yield the input vector $\mathbf{x}(k)$ (the length of the vector equals the number of training or testing steps, i.e. $k \in 1 \cdots N_I$). For a one step ahead x-to-x prediction task the vector $\mathbf{x}(k)$ is the input, i.e. $j_1(k) = \mathbf{x}(k)$ and $N_J = 1$, and $\mathbf{o}(k) = \mathbf{x}(k+1)$ is the target. For cross prediction the target is $\mathbf{o}(k) = \mathbf{z}(k+1)$. It is noted that the sampling step has an impact both on the difficulty of the task and on its memory requirements[54,96,97]. Our focus is on the interrelation between the bifurcation structure and the performance, which is why mainly only one task is used for the discussion (other task have been performed to ensure that the results are robust and are shown in Supplementary Note 2).

We precede the training and testing phases with input buffers (washout phases) in which the reservoir is fed with input. Further, we average over multiple random input masks before determining a performance value (10 masks in two dimensional scans and 30 masks in 1-dimensional scans). The standard deviation of the distribution over the different masks defines the error (see error bars in Figs. 2d and 3c.

Data availability

The numerical data used for this study have been generated using custom code and are not publicly available. They can be reproduced using the code (see code availability statement).

Code availability

The code can be provided by the corresponding author after reasonable request.

Received: 15 July 2024; Accepted: 28 October 2024;
Published online: 14 November 2024

References

1. Eberhardt, S. P., Daud, T., Kerns, D. A., Brown, T. X. & Thakoor, A. P. Competitive neural architecture for hardware solution to the assignment problem. *Neural Netw.* **4**, 431 (1991).
2. Siegelmann, H. T. & Sontag, E. D. Analog computation via neural networks. *Theor. Comp. Sci.* **131**, 331 (1994).
3. Maass, W., Natschläger, T. & Markram, H. Real-time computing without stable states: A new framework for neural computation based on perturbations. *Neural. Comput.* **14**, 2531 (2002).
4. Jaeger, H. *The 'echo state' approach to analysing and training recurrent neural networks*, GMD Report 148 (GMD - German National Research Institute for Computer Science, 2001).
5. Verstraeten, D., Schrauwen, B., D'Haene, M. & Stroobandt, D. An experimental unification of reservoir computing methods. *Neural Networks* **20**, 391 (2007).
6. Zhang, H. & Vargas, D. V. A survey on reservoir computing and its interdisciplinary applications beyond traditional machine learning. *IEEE Access* **11**, 81033 (2023).
7. Genty, G. et al. Machine learning and applications in ultrafast photonics. *Nat. Photonics* **15**, 91 (2021).
8. Brunner, D., Soriano, M. C. & Van der Sande, G. *Photonic Reservoir Computing, Optical Recurrent Neural Networks* (De Gruyter, 2019).
9. Appeltant, L. et al. Information processing using a single dynamical node as complex system. *Nat. Commun.* **2**, 468 (2011).
10. Lindemann, M., Pusch, T., Michalzik, R., Gerhardt, N. C. & Hofmann, M. R. Frequency tuning of polarization oscillations: Toward high-speed spin-lasers. *Appl. Phys. Lett.* **108**, 042404 (2016).
11. Torre, M. S. et al. High frequency continuous birefringence-induced oscillations in spin-polarized vertical-cavity surface-emitting lasers. *Opt. Lett.* **42**, 1628 (2017).
12. Lindemann, M. et al. Ultrafast spin-lasers. *Nature* **568**, 212 (2019).
13. Tselios, C., Georgiou, P., Politi, C., Hurtado, A. & Alexandropoulos, D. Polarization modulation in quantum-dot spin-vcsels for ultrafast data transmission. *IEEE J. Quantum Electron.* **59**, 2400308 (2023).
14. Skalli, A. et al. Photonic neuromorphic computing using vertical cavity semiconductor lasers. *Opt. Mater. Express* **12**, 2395 (2022).
15. Chen, Z. et al. Deep learning with coherent vcsel neural networks. *Nat. Photonics* **17**, 723 (2023).
16. Gauthier, D. J., Bollt, E. M., Griffith, A. & Barbosa, W. A. S. Next generation reservoir computing. *Nat. Commun.* **12**, 5564 (2021).

17. Paquot, Y. et al. Optoelectronic reservoir computing. *Sci. Rep.* **2**, 287 (2012).
18. Larger, L. et al. Photonic information processing beyond turing: an optoelectronic implementation of reservoir computing. *Opt. Express* **20**, 3241 (2012).
19. Brunner, D., Soriano, M. C., Mirasso, C. R. & Fischer, I. Parallel photonic information processing at gigabyte per second data rates using transient states. *Nat. Commun.* **4**, 1364 (2013).
20. Chembo, Y. K. Machine learning based on reservoir computing with time-delayed optoelectronic and photonic systems. *Chaos* **30**, 013111 (2020).
21. Dambre, J., Verstraeten, D., Schrauwen, B. & Massar, S. Information processing capacity of dynamical systems. *Sci. Rep.* **2**, 514 (2012).
22. Grigoryeva, L., Henriques, J., Larger, L. & Ortega, J.-P. Optimal nonlinear information processing capacity in delay-based reservoir computers. *Sci. Rep.* **5**, 12858 (2015).
23. Ortín, S. & Pesquera, L. Reservoir computing with an ensemble of time-delay reservoirs. *Cognitive Computation* **9**, 327 (2017).
24. Röhm, A., Jaurigue, L. & Lüdge, K. Reservoir computing using laser networks. *IEEE J. Sel. Top. Quantum Electron.* **26**, 7700108 (2019).
25. Stelzer, F., Röhm, A., Lüdge, K. & Yanchuk, S. Performance boost of time-delay reservoir computing by non-resonant clock cycle. *Neural Netw.* **124**, 158 (2020).
26. Köster, F., Yanchuk, S. & Lüdge, K. Insight into delay based reservoir computing via eigenvalue analysis. *J. Phys. Photonics* **3**, 024011 (2021).
27. Köster, F., Yanchuk, S. & Lüdge, K. Master memory function for delay-based reservoir computers with single-variable dynamics. *IEEE Trans. Neural Netw. Learn. Syst.* **35**, 7712 (2024).
28. Carroll, T. L. & Hart, J. D. Time shifts to reduce the size of reservoir computers. *Chaos* **32**, 083122 (2022).
29. Hülser, T., Köster, F., Lüdge, K. & Jaurigue, L. Deriving task specific performance from the information processing capacity of a reservoir computer. *Nanophotonics* **12**, 937 (2023).
30. Nakayama, J., Kanno, K. & Uchida, A. Laser dynamical reservoir computing with consistency: an approach of a chaos mask signal. *Opt. Express* **24**, 8679 (2016).
31. Bueno, J., Brunner, D., Soriano, M. C. & Fischer, I. Conditions for reservoir computing performance using semiconductor lasers with delayed optical feedback. *Opt. Express* **25**, 2401 (2017).
32. Vatin, J., Rontani, D. & Sciamanna, M. Experimental reservoir computing using vcsel polarization dynamics. *Opt. Express* **27**, 18579 (2019).
33. Bueno, J., Robertson, J., Hejda, M. & Hurtado, A. Comprehensive performance analysis of a vcsel-based photonic reservoir computer. *IEEE Photon. Technol. Lett.* **33**, 920 (2021).
34. Nguimdo, R. M. & Erneux, T. Enhanced performances of a photonic reservoir computer based on a single delayed quantum cascade laser. *Opt. Lett.* **44**, 49 (2019).
35. Li, X. et al. Performance-enhanced time-delayed photonic reservoir computing system using a reflective semiconductor optical amplifier. *Opt. Express* **31**, 28764 (2023).
36. Gu, B. L., Xiang, S. Y., Guo, X. X., Zheng, D. Z. & Hao, Y. Enhanced prediction performance of a time-delay reservoir computing system based on a vcsel by dual-training method. *Opt. Express* **30**, 30779 (2022).
37. Guo, X. X. et al. Experimental demonstration of modulation format recognition using reservoir computing based on vcsel with gradient-like boosting. *IEEE J. Sel. Top. Quantum Electron.* **29**, 7600808 (2023).
38. Yue, D., Hou, Y., Hu, C., Zang, C. & Kou, Y. Chinese herbal medicine recognition using a vcsel-based time-delay reservoir computing system. *IEEE Photonics Journal* **15**, 1 (2023).
39. Vatin, J., Rontani, D. & Sciamanna, M. Enhanced performance of a reservoir computer using polarization dynamics in vcsels. *Opt. Lett.* **43**, 4497 (2018).
40. Tan, X., Hou, Y. S., Wu, Z. M. & Xia, G. Q. Parallel information processing by a reservoir computing system based on a vcsel subject to double optical feedback and optical injection. *Opt. Express* **27**, 26070 (2019).
41. Guo, X. X. et al. Polarization multiplexing reservoir computing based on a VCSEL with polarized optical feedback. *IEEE J. Sel. Top. Quantum Electron.* **26**, 1700109 (2020).
42. Harkhoe, K., Verschaffelt, G. & Van der Sande, G. Neuro-inspired computing with spin-vcsels. *Appl. Sci.* **11**, 4232 (2021).
43. Yang, Y., Zhou, P., Mu, P. & Li, N. Time-delayed reservoir computing based on an optically pumped spin vcsel for high-speed processing. *Nonlinear Dyn.* **107**, 2619–2632 (2022).
44. Skontranis, M., Sarantoglou, G., Bogris, A. & Mesaritakis, C. Time-delayed reservoir computing based on a dual-waveband quantum-dot spin polarized vertical cavity surface-emitting laser. *Opt. Mater. Express* **12**, 4047 (2022).
45. Zhou, H. X. et al. Photonic convolutional reservoir computing based on vcsel with multiple optical injections. *Opt. Commun.* **545**, 129711 (2023).
46. Huang, Y., Zhou, P., Yang, Y. G., Cai, D. Y. & Li, N. Q. G. Enhanced performance of reservoir computing using multiple self-injection and mutual injection vcsels. *IEEE J. Sel. Top. Quantum Electron.* **29**, 1700109 (2023).
47. Zhang, M., Liang, Z. & Huang, Z. Hardware optimization for photonic time-delay reservoir computer dynamics. *Neuromorph. Comput. Eng.* **3**, 014008 (2023).
48. Goldmann, M., Köster, F., Lüdge, K. & Yanchuk, S. Deep time-delay reservoir computing: Dynamics and memory capacity. *Chaos,* **30**, 093124 (2020).
49. Grigoryeva, L., Hart, A. G. & Ortega, J.-P. Chaos on compact manifolds: Differentiable synchronizations beyond the takens theorem. *Phys. Rev. E* **103**, 062204 (2021).
50. Carroll, T. L. Do reservoir computers work best at the edge of chaos? *Chaos* **30**, 121109 (2020).
51. Marquez, B. A., Suarez-Vargas, J. & Shastri, B. J. Takens-inspired neuromorphic processor: A downsizing tool for random recurrent neural networks via feature extraction. *Phys. Rev. Res.* **1**, 033030 (2019).
52. Sakemi, Y., Morino, K., Leleu, T. & Aihara, K. Model-size reduction for reservoir computing by concatenating internal states through time. *Sci. Rep.* **10**, 21794 (2020).
53. Hart, J. D., Sorrentino, F. & Carroll, T. L. Time-shift selection for reservoir computing using a rank-revealing QR algorithm. *Chaos* **33**, 043133 (2023).
54. Jaurigue, L. & Lüdge, K. Reducing reservoir computer hyperparameter dependence by external timescale tailoring. *Neuromorph. Comput. Eng.* **4**, 014001 (2024).
55. Parlitz, U. Learning from the past: reservoir computing using delayed variables. *Front. Appl. Math. Stat*. **10**, https://doi.org/10.3389/fams.2024.1221051 (2024).
56. Jaurigue, L., Robertson, E., Wolters, J. & Lüdge, K. Reservoir computing with delayed input for fast and easy optimization. *Entropy* **23**, 1560 (2021).
57. Ma, H., Prosperino, D. & Räth, C. A novel approach to minimal reservoir computing. *Sci. Rep.* **13**, 12970 (2023).
58. Köster, F., Patel, D., Wikner, A., Jaurigue, L. & Lüdge, K. Data-informed reservoir computing for efficient time-series prediction. *Chaos* **33**, 073109 (2023).
59. Duncan, D. & Räth, C. Optimizing the combination of data-driven and model-based elements in hybrid reservoir computing. *Chaos* **33**, 103109 (2023).

60. Jaurigue, J., Robertson, J., Hurtado, A., Jaurigue, L. & Lüdge, K. Total recall: Post-processing methods for delay-embedding and feature scaling of reservoir computers. *Commun. Eng*. in the press (2024).
61. Lang, R. & Kobayashi, K. External optical feedback effects on semiconductor injection laser properties. *IEEE J. Quantum Electron.* **16**, 347 (1980).
62. Nizette, M. & Erneux, T. Stability of injection-locked cw-emitting external-cavity semiconductor lasers. *IEEE J. Sel. Top. Quantum Electron.* **10**, 961 (2004).
63. Otto, C., Lüdge, K. & Schöll, E. Modeling quantum dot lasers with optical feedback: sensitivity of bifurcation scenarios. *Phys. Status Solidi B* **247**, 829 (2010).
64. Lüdge, K. & Lingnau, B. In *Laser dynamics and delayed feedback* 2nd ed. Encyclopedia of Complexity and Systems Science Series 31 (Springer Nature, 2020). https://doi.org/10.1007/978-3-642-27737-5_729-1.
65. Köster, F., Lingnau, B., Krimlowski, A., Hövel, P. & Lüdge, K. Collective coherence resonance in networks of optical neurons. *Phys. Status Solidi B* **2021**, 2100345 (2021).
66. Oliverio, L., Rontani, D. & Sciamanna, M. High-resolution dynamic consistency analysis of photonic time-delay reservoir computer. *Opt. Lett.* **48**, 2716 (2023).
67. Hülser, T., Köster, F., Jaurigue, L. & Lüdge, K. Role of delay-times in delay-based photonic reservoir computing. *Opt. Mater. Express* **12**, 1214 (2022).
68. Rottschäfer, V. & Krauskopf, B. The ECM-backbone of the Lang-Kobayashi equations: A geometric picture. *Int. J. Bifurc. Chaos* **17**, 1575 (2007).
69. Hausen, J. et al. Feedback induced locking in semiconductor lasers with strong amplitude-phase coupling. *Phys. Rev. A* **103**, 043511 (2021).
70. Borghi, M., Biasi, S. & Pavesi, L. Reservoir computing based on a silicon microring and time multiplexing for binary and analog operations. *Sci. Rep.* **11**, 15642 (2021).
71. Donati, G., Mirasso, C. R., Mancinelli, M., Pavesi, L. & Argyris, A. Microring resonators with external optical feedback for time delay reservoir computing. *Opt. Express* **30**, 522 (2022).
72. Abdalla, M. et al. Minimum complexity integrated photonic architecture for delay-based reservoir computing. *Opt. Express* **31**, 11610 (2023).
73. Huang, L. & Yao, J. Multi-task photonic time-delay reservoir computing based on polarization modulation. *Opt. Lett.* **47**, 6464 (2022).
74. Köster, F., Ehlert, D. & Lüdge, K. Limitations of the recall capabilities in delay based reservoir computing systems. *Cogn. Comput*. **15**, 1419 (2020).
75. Lingnau, B., Dillane, M., O'Callaghan, J., Corbett, B. & Kelleher, B. Multimode dynamics and modelling of free-running and optically injected Fabry-Pérot quantum-dot lasers. *Phys. Rev. A* **100**, 063837 (2019).
76. Nizette, M. & Erneux, T. Bifurcations of injection-locked semiconductor lasers subject to optical feedback. *Proc. of SPIE* **5452**, https://doi.org/10.1117/12.545614 (2004).
77. Wieczorek, S., Krauskopf, B., Simpson, T. B. & Lenstra, D. The dynamical complexity of optically injected semiconductor lasers. *Phys. Rep.* **416**, 1 (2005).
78. Globisch, B., Otto, C., Schöll, E. & Lüdge, K. Influence of carrier lifetimes on the dynamical behavior of quantum-dot lasers subject to optical feedback. *Phys. Rev. E* **86**, 046201 (2012).
79. Erneux, T., Gavrielides, A. & Sciamanna, M. Stable microwave oscillations due to external-cavity-mode beating in laser diodes subject to optical feedback. *Phys. Rev. E* **66**, 033809 (2002).
80. Erneux, T. *Applied delay differential equations* (Springer, 2009).
81. Miguel, M. S., Feng, Q. & Moloney, J. V. Light-polarization dynamics in surface-emitting semiconductor lasers. *Phys. Rev. A* **52**, 1728 (1995).
82. Martin-Regalado, J., Prati, F., San Miguel, M. & Abraham, N. B. Polarization properties of vertical-cavity surface-emitting lasers. *IEEE J. Quantum Electron.* **33**, 765 (1997).
83. Adams, M., Li, N., Cemlyn, B., Susanto, H. & Henning, I. Algebraic expressions for the polarisation response of spin-vcsels. *Sem. Sci. Techno.* **33**, 064002 (2018).
84. Li, N., Alexandropoulos, D., Susanto, H., Henning, I. & Adams, M. J. Stability analysis of Quantum-Dot spin-VCSELs. *Electronics* **5**, 83 (2016).
85. Song, T. et al. Numerical analysis of nonlinear dynamics based on spin-vcsels with optical feedback. *Photonics* **8**, 10 (2021).
86. Pieroux, D., Erneux, T., Haegeman, B., Engelborghs, K. & Roose, D. Bridges of periodic solutions and tori in semiconductor lasers subject to delay. *Phys. Rev. Lett.* **87**, 193901 (2001).
87. Heil, T. et al. Delay dynamics of semiconductor lasers with short external cavities: Bifurcation scenarios and mechanisms. *Phys. Rev. E* **67**, 066214 (2003).
88. Pausch, J. et al. Optically injected quantum dot lasers - impact of nonlinear carrier lifetimes on frequency locking dynamics. *New J. Phys.* **14**, 053018 (2012).
89. Lingnau, B., Schicke, D., Eichelmann, M. & Lüdge, K. Dynamic signatures of mode competition in optically injected high-β lasers. *New J. Phys.* **22**, 073052 (2020).
90. Valagiannopoulos, C. & Kovanis, V. Injection-locked photonic oscillators: Legacy results and future applications. *IEEE Antennas Propag. Mag.* **63**, 51 (2021).
91. Erneux, T., Kovanis, V. & Gavrielides, A. Nonlinear dynamics of an injected quantum cascade laser. *Phys. Rev. E* **88**, 032907 (2013).
92. Pochet, M. C., Naderi, N. A., Kovanis, V. & Lester, L. F. Modeling the dynamic response of an optically-injected nanostructure diode laser. *IEEE J. Quantum Electron.* **47**, 827 (2011).
93. Owen-Newns, D., Robertson, J., Hejda, M. & Hurtado, A. Photonic spiking neural networks with highly efficient training protocols for ultrafast neuromorphic computing systems. *Intell. Comput.* **2**, 0031 (2023).
94. Jaurigue, L. Chaotic attractor reconstruction using small reservoirs-the influence of topology. *Mach. Learn. Sci. Technol.* **5**, 035058 (2024).
95. Lorenz, E. N. Deterministic nonperiodic flow. *J. Atmos. Sci.* **20**, 130 (1963).
96. Tsuchiyama, K., Röhm, A., Mihana, T., Horisaki, R. & Naruse, M. Effect of temporal resolution on the reproduction of chaotic dynamics via reservoir computing. *Chaos* **33**, 063145 (2023).
97. Xie, Q., Yan, Z., Zhao, H., Gao, J. & Xiao, J. Large sampling intervals for learning and predicting chaotic systems with reservoir computing. *J. Phys. A Math. Theor.* **57**, 295702 (2024).

Acknowledgements

This work was supported by the German research Foundation (DFG) with Project No. 411803875 and from the European Union's Horizon 2020 programme under grant agreement number 101129904 (SPIKEPro).

Author contributions

L.M., J.J. and K.L. performed the numerical simulations. L.J. and K.L. initiated and supervised the project. All authors contributed in writing and discussing the manuscript.

Funding

Open Access funding enabled and organized by Projekt DEAL.

Competing interests
The authors declare no competing interests.

Additional information
Supplementary information The online version contains supplementary material available at https://doi.org/10.1038/s42005-024-01858-5.

Correspondence and requests for materials should be addressed to Lina C. Jaurigue or Kathy Lüdge.

Peer review information *Communications Physics* thanks the anonymous reviewers for their contribution to the peer review of this work. A peer review file is available.